

# TasNet: Surpassing Ideal Time-Frequency Masking for Speech Separation

Yi Luo, Nima Mesgarani

**Abstract**—Robust speech processing in multitalker acoustic environments requires automatic speech separation. While single-channel, speaker-independent speech separation methods have recently seen great progress, the accuracy, latency, and computational cost of speech separation remain insufficient. The majority of the previous methods have formulated the separation problem through the time-frequency representation of the mixed signal, which has several drawbacks, including the decoupling of the phase and magnitude of the signal, the suboptimality of spectrogram representations for speech separation, and the long latency in calculating the spectrogram. To address these shortcomings, we propose the time-domain audio separation network (TasNet), which is a deep learning autoencoder framework for time-domain speech separation. TasNet uses a convolutional encoder to create a representation of the signal that is optimized for extracting individual speakers. Speaker extraction is achieved by applying a weighting function (mask) to the encoder output. The modified encoder representation is then inverted to the sound waveform using a linear decoder. The masks are found using a temporal convolutional network consisting of dilated convolutions, which allow the network to model the long-term dependencies of the speech signal. This end-to-end speech separation algorithm significantly outperforms previous time-frequency methods in terms of separating speakers in mixed audio, even when compared to the separation accuracy achieved with the ideal time-frequency mask of the speakers. In addition, TasNet has a smaller model size and a shorter minimum latency, making it a suitable solution for both offline and real-time speech separation applications. This study therefore represents a major step toward actualizing speech separation for real-world speech processing technologies.

**Index Terms**—Source separation, single-channel, time-domain, deep learning, real-time

## I. INTRODUCTION

Robust speech processing in real-world acoustic environments often requires automatic speech separation. For example, successfully recognizing speech in multitalker conditions first requires the separation of individual speakers in the mixture sound before identifying a target speaker or recognizing target speech. Because of the importance of this research topic for speech processing technologies, numerous methods have been proposed for solving this problem. However, the accuracy of speech separation, particularly for unseen speakers, remains inadequate. Most previous speech separation approaches have been formulated in the time-frequency (T-F, or spectrogram) representation of the mixture signal, which is estimated from the waveform using the short-time Fourier transform (STFT) [1]. Speech separation methods in the T-F domain aim to approximate the cleaned spectrogram of the individual sources from the mixture spectrogram. This process can be performed by directly approximating the spectrogram representation of each source from the mixture using nonlinear

regression techniques, where the clean source spectrograms are used as the training target [2], [3], [4]. Alternatively, a weighting function (mask) can be estimated for each source to multiply each T-F bin in the mixture spectrogram to recover the individual sources. In recent years, deep learning has greatly advanced the performance of time-frequency masking methods by increasing the accuracy of the mask estimation [5], [6], [7], [8], [9], [10], [11]. In both the direct method and the mask estimation method, the waveform of each source is calculated using the inverse short-time Fourier transform (iSTFT) of the estimated magnitude spectrogram of each source together with either the original or the modified phase of the mixture sound. While time-frequency masking remains the most commonly used method for speech separation, this method has several shortcomings. First, STFT is a generic signal transformation that is not necessarily optimal for speech separation. Second, accurate reconstruction of the phase of the clean sources is a nontrivial problem, and the erroneous estimation of the phase introduces an upper bound on the accuracy of the reconstructed audio. This issue is evident by the imperfect reconstruction accuracy of the sources even when the actual (ideal) clean magnitude spectrograms are applied to the mixture. Although methods for phase reconstruction can be applied to alleviate this issue [12], [13], the performance of the method remains suboptimal. Third, successful separation from the time-frequency representation requires a high-resolution frequency decomposition of the mixture signal, which requires a long temporal window for the calculation of STFT. This requirement increases the minimum latency of the system, which limits its applicability in real-time, low-latency applications such as in telecommunication and hearable devices. For example, the window length of STFT in most speech separation systems is at least 32 ms [5], [6], [7] and is even greater in music separation applications, which require an even higher resolution spectrogram (higher than 90 ms) [14], [15]. Because these issues arise from formulating the separation problem in the time-frequency domain, a sensible approach is to avoid decoupling the magnitude and the phase of the sound by directly formulating the separation in the time domain. Previous studies have explored the feasibility of time-domain speech separation through methods such as independent component analysis (ICA) [16] and time-domain nonnegative matrix factorization (NMF) [17]. However, the performance of these systems has not been comparable with the performance of time-frequency approaches, particularly in terms of their ability to scale and generalize to large data. On the other hand, a few recent studies have explored deep learning for time-domain speech separation, with mixed

success [18], [19]. One such method is the time-domain audio separation network (TasNet) [20]. In TasNet, the mixture waveform is modeled with a convolutional autoencoder, which consists of an encoder with a nonnegativity constraint. This approach eliminates the problems arising from detaching the magnitude and the phase and results in a representation of the mixture sound that can be optimized for speech separation. A linear deconvolution layer serves as a decoder by inverting the encoder output back to the sound waveform. This encoder-decoder framework is similar to the ICA method when a nonnegative mixing matrix is used [21] and to the semi-nonnegative matrix factorization method (semi-NMF) [22], where the basis signals are the parameters of the decoder. The separation step in TasNet is done by finding a weighting function for each source (similar to time-frequency masking) for each of the encoder outputs and at each time step. TasNet outperformed time-frequency speech separation methods in both causal and noncausal implementations, in addition to having a minimum latency of only 6 ms compared to 32 ms for the STFT-based methods [20].

Despite its promising performance, the use of a deep long short-term memory (LSTM) network as the separation module in the original TasNet [20] limited its applicability. First, choosing smaller kernel sizes (i.e. lengths of the waveform segments) in the convolutional autoencoder increases the number of time frames in the encoder output, which makes the training of the LSTMs unmanageable. Second, the large number of parameters in a deep LSTM network increases its computational complexity and limits its applicability to low-resource, low-power platforms such as wearable hearing devices. The third problem is caused by the long temporal dependencies of LSTM networks, which can result in accumulated error and increased sensitivity of the performance to the exact starting point of the mixture waveform.

To alleviate the limitations of TasNet, we propose a fully-convolutional TasNet (Conv-TasNet) that uses stacked dilated 1-D convolutional networks. This method is motivated by the success of temporal convolutional network (TCN) models [23], [24], [25], which allow parallel processing on consecutive frames or segments to speed up the separation process; this also reduces the model size. To further decrease the number of parameters and the computational complexity of the system, we substitute the original convolution operation with depthwise separable convolution [26], [27]. We show that this configuration significantly increases the separation accuracy over the previous LSTM-TasNet. Moreover, the separation accuracy of Conv-TasNet surpasses the performance of ideal time-frequency masks, including the ideal binary mask (IBM [28]), ideal ratio mask (IRM, [29], [30]), and Winener filter-like mask (WFM, [31]).

The rest of the paper is organized as follows. We briefly discuss related work in Section II. We introduce the proposed Conv-TasNet in Section III, describe the experimental procedures in Section IV, and show the experimental results and analysis in Section V. We conclude the paper in Section VI.

## II. RELATED WORK

Time-domain approaches have typically relied on differences in the statistical properties of the sources being separated. These methods model the statistics of the target and interfering sources, which can be used in computational frameworks such as the maximum likelihood estimation (MLE). One notable approach in this category is independent component analysis (ICA) [32], [33], [34]: the target and interfering sources are decomposed into a set of statistically independent basis signals, which enables their separation. The accuracy of ICA-based approaches depends heavily on the fidelity of the estimated basis signals and the statistical separability of the target and interfering sources. This aspect, however, limits their applicability when all the sources are speech signals and therefore have similar statistical properties [35], [36], [37], [38].

Beyond ICA methods, several recent studies have investigated the feasibility of time-domain separation with deep learning [18], [19], [20]. The shared idea in all these systems is to replace the STFT step for feature extraction with a data-driven representation that is jointly optimized with an end-to-end training paradigm. These representations and their inverse transforms can be explicitly designed to replace STFT and iSTFT. Alternatively, feature extraction can be implicitly incorporated into the network architecture, for example by using a convolutional neural network layer (CNN) [39], [40]. These methods are different in how they extract features from the waveform and in terms of the design of the separation module. In [18], a discrete cosine transform (DCT) type convolutional autoencoder is used as the front end, in which the magnitude and phase information are encoded separately. The separation is then performed on the magnitude of the front end, similar to time-frequency masking. In [19], the separation is incorporated into a U-net CNN architecture [41] without explicitly transforming the input into a spectrogram-like representation. [20] uses a convolutional autoencoder with a nonnegativity constraint on the encoder output to replace STFT and its inverse; it reformulates the separation task as a mask estimation problem on the encoder output.

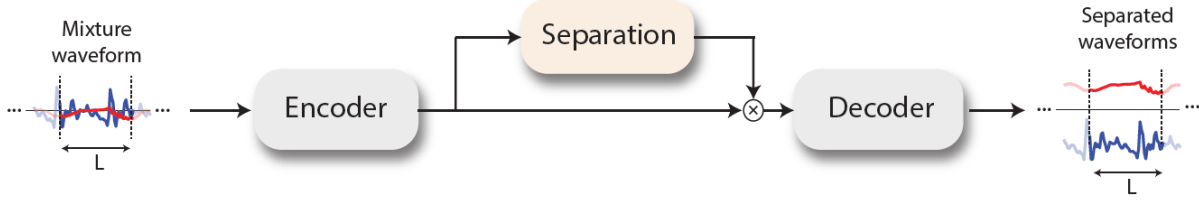
## III. CONVOLUTIONAL TIME-DOMAIN AUDIO SEPARATION NETWORK

The fully-convolutional time-domain audio separation network (Conv-TasNet) consists of three processing stages, as shown in Figure 1 A: encoder, separation, and decoder. First, an encoder module is used to transform short segments of the mixture waveform into their corresponding representations in an intermediate feature space. This representation is then used to estimate a multiplicative function (mask) for each source and for each encoder output at each time step. The source waveforms are then reconstructed by transforming the masked encoder features using a linear decoder module. We describe the details of each stage in this section.

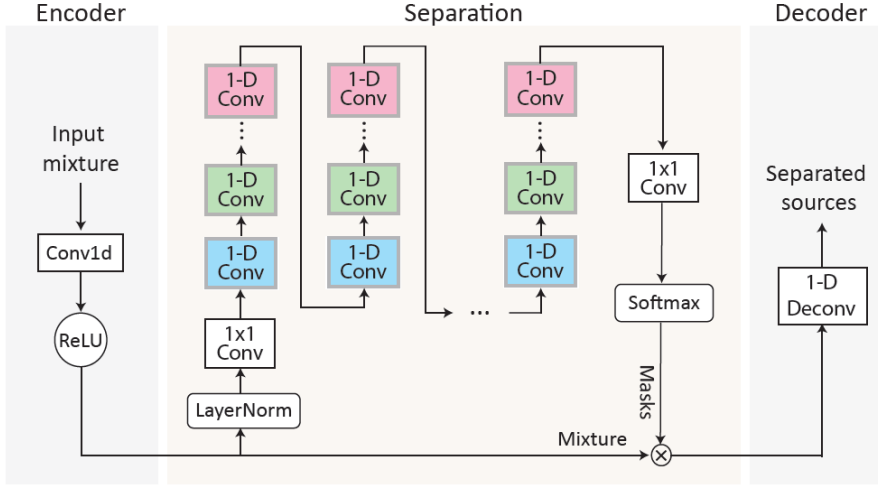
### A. Time-domain speech separation

The problem of single-channel speech separation can be formulated in terms of estimating  $C$  sources  $s_1(t), \dots, s_c(t) \in$

### A. TasNet block diagram



### B. System flowchart



### C. Dilated convolutions

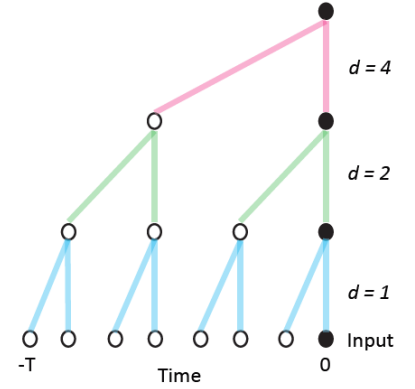


Fig. 1. (A): the block diagram of the TasNet system. An encoder maps a segment of the mixture waveform to a high-dimensional representation and a separation module calculates a multiplicative function (i.e., a mask) for each of the target sources. A decoder reconstructs the source waveforms from the masked features. (B): A flowchart of the proposed system. A 1-D convolutional autoencoder models the waveforms and a dilated convolutional separation module estimates the masks based on the nonnegative encoder output. (C): An example of causal dilated convolution with three kernels of size 2.

$\mathbb{R}^{1 \times T}$ , given the discrete waveform of the mixture  $x(t) \in \mathbb{R}^{1 \times T}$ , where

$$x(t) = \sum_{i=1}^C s_i(t) \quad (1)$$

In time-domain audio separation, we aim to directly estimate  $s_i(t), i = 1, \dots, C$ , from  $x(t)$ .

#### B. Convolutional autoencoder

Each segment of the input mixture sound with length  $L$ ,  $\mathbf{x}_k \in \mathbb{R}^{1 \times L}$  (hereafter  $\mathbf{x}$  for simplicity) where  $k = 1, \dots, \frac{T}{L}$ , is transformed into a nonnegative representation,  $\mathbf{w} \in \mathbb{R}^{1 \times N}$  by a 1-D convolution operation (the index  $k$  is dropped from now on):

$$\mathbf{w} = \text{ReLU}(\mathbf{x} \circledast \mathbf{U}) \quad (2)$$

where  $\mathbf{U} \in \mathbb{R}^{N \times L}$  contains  $N$  vectors (encoder basis functions) with length  $L$  each, and  $\circledast$  denotes the convolution operation.  $\text{ReLU}$  denotes the rectified linear unit activation. The decoder reconstructs the waveform from this representation using a 1-D linear deconvolution operation, which can be defined as a matrix multiplication in this case:

$$\hat{\mathbf{x}} = \mathbf{w} \mathbf{V} \quad (3)$$

where  $\hat{\mathbf{x}} \in \mathbb{R}^{1 \times L}$  is the reconstruction of  $\mathbf{x}$ , and the rows in  $\mathbf{V} \in \mathbb{R}^{N \times L}$  are the decoder basis functions, each with length

$L$ . In the case of overlapping encoder outputs, the overlapping reconstructed segments are summed together to generate the final reconstructions.

#### C. Estimating the separation masks

The separation for each frame is performed by estimating  $C$  vectors (masks)  $\mathbf{m}_i \in \mathbb{R}^{1 \times N}, i = 1, \dots, C$  where  $C$  is the number of speakers in the mixture that is multiplied by the encoder output  $\mathbf{w}$ . The mask vectors  $\mathbf{m}_i$  have the constraint that  $\sum_{i=1}^C \mathbf{m}_i = \mathbf{1}$ , where  $\mathbf{1}$  is the unit vector in  $\mathbb{R}^{1 \times N}$ . The representation of each source,  $\mathbf{d}_i \in \mathbb{R}^{1 \times N}$ , is then calculated by applying the corresponding mask,  $\mathbf{m}_i$ , to the mixture representation  $\mathbf{w}$ :

$$\mathbf{d}_i = \mathbf{w} \odot \mathbf{m}_i \quad (4)$$

The waveform of each source  $\hat{s}_i, i = 1, \dots, C$  is then reconstructed by the decoder:

$$\hat{s}_i = \mathbf{d}_i \mathbf{V} \quad (5)$$

The unit summation constraint that is imposed on the masks guarantees that the reconstructed sources add up to the reconstructed mixture:  $\hat{\mathbf{x}} = \sum_{i=1}^C \hat{s}_i$  since  $\sum_{i=1}^C \mathbf{d}_i = \mathbf{w} \odot \sum_{i=1}^C \mathbf{m}_i = \mathbf{w}$ .

#### D. Convolutional separation module

Motivated by the temporal convolutional network (TCN) [23], [24], [25], we propose a fully convolutional separation module that consists of stacked 1-D dilated convolutional blocks, as shown in Figure 1 B. TCN was proposed as a replacement for RNNs in various tasks [23], [24], [25]. Each layer in a TCN contains a 1-D convolutional block with increasing dilation factors. The dilation factors increase exponentially to ensure a sufficiently large temporal context window to take advantage of the long-range dependencies of the speech signal, as shown in Figure 1 C. In Conv-TasNet,  $M$  convolutional blocks with dilation factors  $1, 2, 4, \dots, 2^{M-1}$  are repeated  $R$  times. The output of the last block in the last repeat is then passed to a  $1 \times 1$  convolutional layer with  $N \times C$  filters followed by a softmax activation function to estimate  $C$  mask vectors for each of the  $C$  target sources. The input to each block is zero padded to ensure the output length is the same as the input.

To further decrease the number of parameters, we utilize depthwise separable convolution ( $S\text{-conv}(\cdot)$ ) to replace standard convolution in each convolutional block. Depthwise separable convolution (also referred to as separable convolution) has proven effective in image processing [26], [27] and neural machine translation tasks [42]. The depthwise separable convolution operator involves two consecutive operations, a *depthwise* convolution ( $D\text{-conv}(\cdot)$ ) followed by a standard convolution with kernel size 1 (*pointwise* convolution,  $1 \times 1\text{-conv}(\cdot)$ ):

$$D\text{-conv}(\mathbf{Y}, \mathbf{K}) = \text{concat}(\mathbf{y}_j \otimes \mathbf{k}_j), j = 1, \dots, N \quad (6)$$

$$S\text{-conv}(\mathbf{Y}, \mathbf{K}, \mathbf{L}) = D\text{-conv}(\mathbf{Y}, \mathbf{K}) \otimes \mathbf{L} \quad (7)$$

where  $\mathbf{Y} \in \mathbb{R}^{G \times M}$  is the input to the  $S\text{-conv}(\cdot)$ ,  $\mathbf{K} \in \mathbb{R}^{G \times P}$  is the convolution kernel with size  $P$ ,  $\mathbf{y}_j \in \mathbb{R}^{1 \times M}$  and  $\mathbf{k}_j \in \mathbb{R}^{1 \times P}$  are the rows of matrices  $\mathbf{Y}$  and  $\mathbf{K}$ , respectively, and  $\mathbf{L} \in \mathbb{R}^{G \times H \times 1}$  is the convolution kernel with size 1. In other words, the  $D\text{-conv}(\cdot)$  operation convolves each row of the input  $Y$  with the corresponding row of matrix  $K$ , and  $1 \times 1\text{-conv}(\cdot)$  is the same as a fully connected linear layer that maps the channel features to a transformed feature space. In comparison with the standard convolution with kernel size  $\mathbf{K} \in \mathbb{R}^{G \times H \times P}$ , depthwise separable convolution only contains  $G \times P + G \times H$  parameters, which decreases the model size by a factor of  $\frac{H \times P}{H + P}$ .

In each 1-D convolutional block, a  $1 \times 1\text{-conv}$  operation is followed by a  $S\text{-conv}$  operation, which is similar to the design in [43]. A nonlinear activation function and a normalization are added after both the first  $1 \times 1\text{-conv}$  and  $D\text{-conv}$  operations, resulting in the architecture shown in Figure 2. The nonlinear activation function is the parametric rectified linear unit (PReLU) [44]:

$$\text{PReLU}(x) = \begin{cases} x, & \text{if } x \geq 0 \\ \alpha x, & \text{otherwise} \end{cases} \quad (8)$$

where  $\alpha \in \mathbb{R}$  is a trainable scalar controlling the negative slope of the rectifier. An identity residual connection [45] is added between the input and output of each convolutional block (2). At the beginning of the separation module, a linear

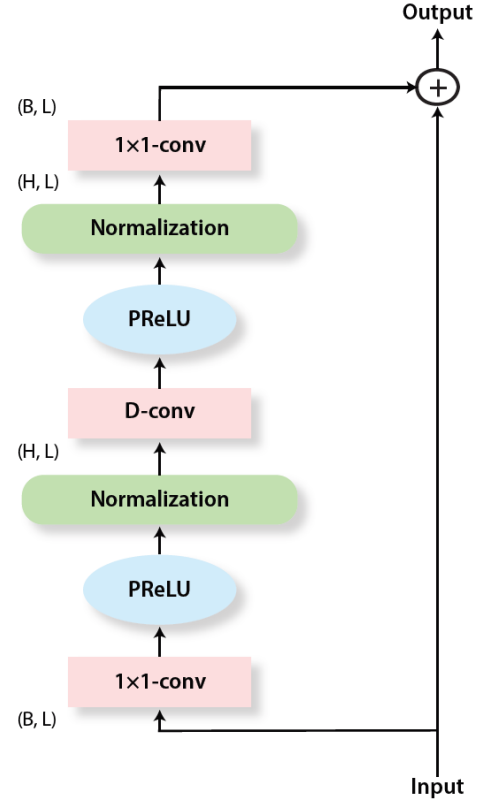


Fig. 2. Each 1-D convolutional block consists of a  $1 \times 1\text{-conv}$  operation followed by a  $S\text{-conv}$  operation, with nonlinear activation function (PReLU) and normalization added between each two convolution operations.

$1 \times 1\text{-conv}$  block is added as a bottleneck layer. This block determines the number of channels in the input and output of the subsequent convolutional blocks. For instance, if the linear bottleneck layer has  $B$  channels, then for a convolutional block with  $H$  channels and kernel size  $P$ , the size of the kernel in the first  $1 \times 1\text{-conv}$  block, the first  $D\text{-conv}$  block and the last  $1 \times 1\text{-conv}$  block should be  $\mathbf{O} \in \mathbb{R}^{B \times H \times 1}$ ,  $\mathbf{K} \in \mathbb{R}^{H \times P}$  and  $\mathbf{L} \in \mathbb{R}^{H \times B \times 1}$ , respectively.

#### E. Normalization methods

We found that the choice of the normalization technique in the convolutional blocks significantly impacts the performance. We used three different normalization schemes: channel-wise layer normalization (cLN), global layer normalization (gLN), and batch normalization (BN).

Channel-wise layer normalization (cLN) is similar to the standard layer normalization operation in sequence modeling [46], which is applied to each segment  $k$  independently:

$$\text{cLN}(\mathbf{y}_k) = \frac{\mathbf{y}_k - E[\mathbf{y}_k]}{\sqrt{\text{Var}(\mathbf{y}_k) + \epsilon}} \odot \gamma + \beta \quad (9)$$

$$E[\mathbf{y}_k] = \frac{1}{N} \sum_N \mathbf{y}_k \quad (10)$$

$$\text{Var}(\mathbf{y}_k) = \frac{1}{N} \sum_N (\mathbf{y}_k - E[\mathbf{y}_k])^2 \quad (11)$$

where  $\mathbf{y}_k \in \mathbb{R}^{N \times 1}$  is the  $k_{th}$  segment of the sequence  $\mathbf{Y}$ , and  $\gamma, \beta \in \mathbb{R}^{N \times 1}$  are trainable parameters. To ensure that the

separation module is invariant to change in the scale of the input, cLN is always applied to the input of the separation module (i.e. the encoder output  $\mathbf{w}$ ):  $\hat{\mathbf{w}} = cLN(\mathbf{w})$ . In the 1-D convolutional blocks, cLN is suitable for both the causal and noncausal configurations.

In global layer normalization (gLN), each feature is normalized over both the channel and the time dimension:

$$gLN(\mathbf{Y}) = \frac{\mathbf{Y} - E[\mathbf{Y}]}{\sqrt{Var(\mathbf{Y}) + \epsilon}} \odot \gamma + \beta \quad (12)$$

$$E[\mathbf{Y}] = \frac{1}{NT} \sum_{NT} \mathbf{Y} \quad (13)$$

$$Var(\mathbf{Y}) = \frac{1}{NT} \sum_{NT} (\mathbf{Y} - E[\mathbf{Y}])^2 \quad (14)$$

where  $\gamma, \beta \in \mathbb{R}^{N \times 1}$  are trainable parameters. Although the normalization is performed globally, the rescaling and recentering by  $\gamma$  and  $\beta$  are performed independently for each time step. Because gLN uses the information from the entire utterance, it can only be used for noncausal implementation.

Batch normalization (BN) [47] can also be applied along the time dimension. Note that the calculation of mean and variance during the training phase requires the entire utterance (i.e. noncausal), but during testing, BN can be used in both the causal and noncausal implementations since the mean and the variance are calculated during the training phase and are subsequently fixed during the test. We will compare the effects of different normalization methods on the performance in section V-A.

## IV. EXPERIMENTAL PROCEDURES

### A. Dataset

We evaluated our system on a two-speaker speech separation problem using the WSJ0-2mix and WSJ0-3mix datasets [48]. Thirty hours of training and 10 hours of validation data are generated from speakers in `si_tr_s` from the datasets. The speech mixtures are generated by randomly selecting utterances from different speakers in the Wall Street Journal dataset (WSJ0) and mixing them at random signal-to-noise ratios (SNR) between -2.5 dB and 2.5 dB. A five-hour evaluation set is generated in the same way using utterances from 16 unseen speakers in `si_dt_05` and `si_et_05`. The scripts for creating the dataset can be found at [49]. All the waveforms are resampled at 8 kHz.

### B. Estimating the hyperparameters

The networks are trained for 100 epochs on 4-second long segments. The initial learning rate is set to  $1e^{-2}$  or  $1e^{-3}$ , depending on the model configuration, and is halved if the accuracy of validation set is not improved in 3 consecutive epochs. Adam [50] is used as the optimizer. A 50% stride size is used in the convolutional autoencoder (i.e. 50% overlap between consecutive frames). The hyperparameters of the network are shown in table I.

TABLE I  
HYPERPARAMETERS OF THE NETWORK.

Symbol	Description
$N$	Number of filters in autoencoder
$L$	Length of the filters (in samples)
$B$	Number of channels in bottleneck $1 \times 1$ -conv block
$H$	Number of channels in convolutional blocks
$P$	Kernel size in convolutional blocks
$X$	Number of convolutional blocks in each repeat
$R$	Number of repeats

### C. Training objective

The objective function for training the end-to-end system is the scale-invariant source-to-noise ratio (SI-SNR), which has commonly been used instead of the standard source-to-distortion ratio (SDR) [51] [5], [8]. SI-SNR is defined as:

$$\begin{cases} \mathbf{s}_{target} := \frac{\langle \hat{\mathbf{s}}, \mathbf{s} \rangle \mathbf{s}}{\|\mathbf{s}\|^2} \\ \mathbf{e}_{noise} := \hat{\mathbf{s}} - \mathbf{s}_{target} \\ \text{SI-SNR} := 10 \log_{10} \frac{\|\mathbf{s}_{target}\|^2}{\|\mathbf{e}_{noise}\|^2} \end{cases} \quad (15)$$

where  $\hat{\mathbf{s}} \in \mathbb{R}^{1 \times T}$  and  $\mathbf{s} \in \mathbb{R}^{1 \times T}$  are the estimated and original clean sources, respectively, and  $\|\mathbf{s}\|^2 = \langle \mathbf{s}, \mathbf{s} \rangle$  denotes the signal power. Scale invariance is ensured by normalizing  $\hat{\mathbf{s}}$  and  $\mathbf{s}$  to zero-mean prior to the calculation. Permutation invariant training (PIT) is applied during training to address the source permutation problem [6].

### D. Evaluation metrics

We report the scale-invariant signal-to-noise ratio (SI-SNR), signal-to-distortion ratio (SDR) [51], and perceptual evaluation of speech quality score (PESQ) [52] as objective measures of speech separation accuracy. SI-SNR is defined in equation 15.

### E. Comparison with ideal time-frequency masks

Following the common configurations in [5], [8], [6], the ideal time-frequency masks were calculated using an STFT with a 32 ms window size and 8 ms hop size with a Hanning window. The ideal masks include the ideal binary mask (IBM), ideal ratio mask (IRM), and Wiener filter mask (WFM), which are defined for source  $i$  as:

$$IBM_i(f, t) = \begin{cases} 1, & |\mathcal{S}_i(f, t)| > |\mathcal{S}_{j \neq i}(f, t)| \\ 0, & \text{otherwise} \end{cases} \quad (16)$$

$$IRM_i(f, t) = \frac{|\mathcal{S}_i(f, t)|}{\sum_{j=1}^C |\mathcal{S}_j(f, t)|} \quad (17)$$

$$WFM_i(f, t) = \frac{|\mathcal{S}_i(f, t)|^2}{\sum_{j=1}^C |\mathcal{S}_j(f, t)|^2} \quad (18)$$

where  $\mathcal{S}_i(f, t) \in \mathbb{C}^{F \times T}$  are the complex-valued spectrograms of the clean sources.

## V. RESULTS

Figure 3 visualizes all the internal variables of TasNet for one example mixture sound with two overlapping speakers

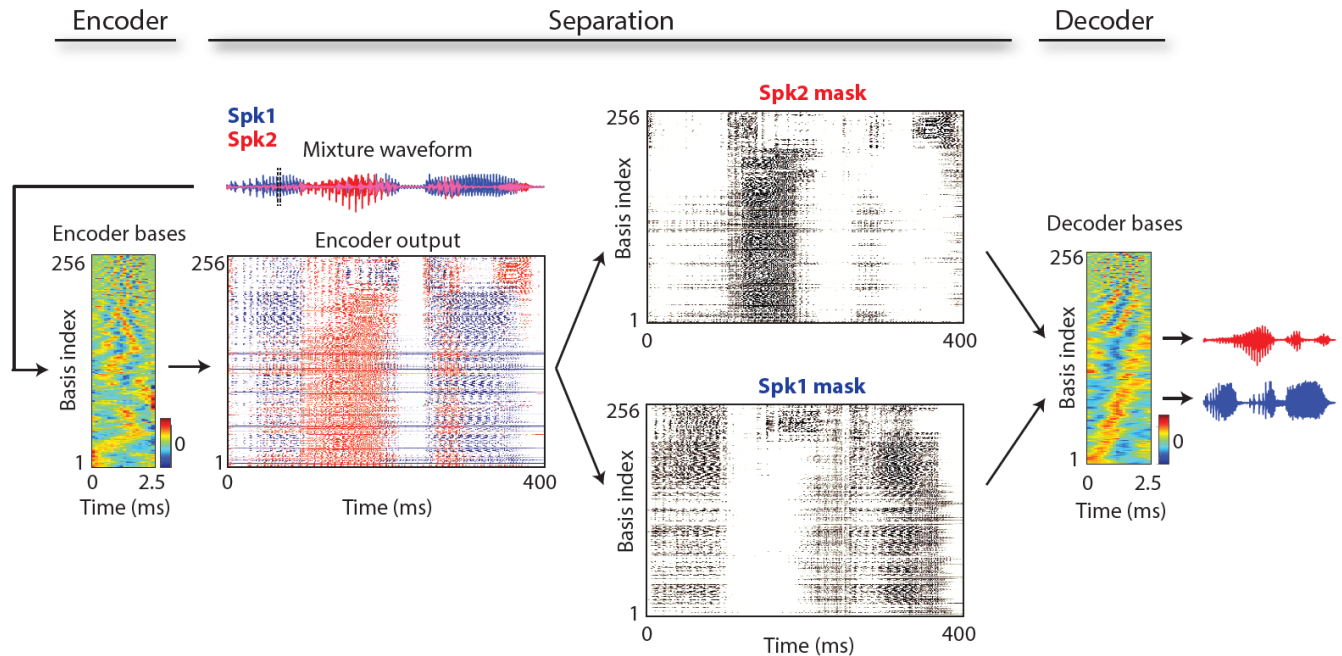


Fig. 3. Visualization of the encoder and decoder basis functions, encoder representation, and source masks for a sample 2-speaker mixture. The speakers are shown in red and blue. The encoder representation is colored according to the power of each speaker at each basis function and point in time. The basis functions are sorted according to their Euclidean similarity and show diversity in frequency and phase tuning.

TABLE II  
THE EFFECT OF DIFFERENT CONFIGURATIONS IN CONV-TASNET.

$N$	$L$	$B$	$H$	$P$	$X$	$R$	Normali- zation	Causal	Receptive field(s)	SI-SNRi (dB)	SDRi (dB)
128	40	64	128	3	7	2	BN	×	1.28	9.2	9.6
128	40	64	256	3	7	2	BN	×	1.28	10.0	10.4
128	40	128	256	3	7	2	BN	×	1.28	10.4	10.8
256	40	128	256	3	7	2	BN	×	1.28	10.5	10.9
256	40	128	512	3	7	2	BN	×	1.28	11.3	11.6
256	40	256	512	3	7	2	BN	×	1.28	11.3	11.7
256	40	256	512	3	6	4	BN	×	1.27	11.7	12.1
256	40	256	512	3	8	2	BN	×	2.56	12.2	12.6
256	40	256	512	3	7	4	BN	×	2.55	12.6	13.0
256	20	256	512	3	8	4	BN	×	2.55	14.3	14.7
256	20	256	512	3	8	4	cLN	×	2.55	14.0	14.4
256	20	256	512	3	8	4	gLN	×	2.55	<b>14.6</b>	<b>15.0</b>
256	20	256	512	3	8	4	BN	✓	2.55	<b>10.8</b>	<b>11.2</b>
256	20	256	512	3	8	4	cLN	✓	2.55	10.5	10.9

(denoted by red and blue). The encoder and decoder basis functions are sorted based on the Euclidean similarity, which is found using an unsupervised clustering algorithm [53]. The basis functions show a diversity of frequency and phase tuning. The representation of the encoder is colored according to the power of each speaker at the corresponding basis output at each time point, demonstrating the sparsity of the encoder representation. As can be seen in Figure 3, the estimated masks for each of the two speakers highly resemble their encoder representations, which allows for the suppression of the encoder outputs that correspond to the interfering speaker and the extraction of the target speaker in each mask. The separated waveforms for the two speakers are estimated by the

linear decoder, whose basis functions are shown in Figure 3. The separated waveforms are shown on the right.

#### A. Optimizing the network parameters

We first evaluate the performance of Conv-TasNet on two speaker separation tasks as a function of different network parameters. Table II shows the performance of the systems with different parameters, where the following observations become evident:

- (i) With the same configuration of the autoencoder and the channels in the linear  $1 \times 1$ -conv bottleneck layer  $B$ , more channels in the convolutional blocks  $H$  leads

to better performance, indicating the importance of a separation module with sufficient computational capacity.

- (ii) With the same configuration of the autoencoder and the convolutional blocks, more channels in the linear  $1 \times 1$ -conv bottleneck layer  $B$  leads to better performance, confirming again the notion that the separation module should have high modeling capacity.
- (iii) With the same configuration of the separation module, more filters in the autoencoder  $N$  leads to minor improvement. This result suggests an upper bound for the utility of an overcomplete encoder representation, beyond which the separation does not improve.
- (iv) With the same configuration of the autoencoder and channels in the separation module ( $B$  and  $H$ ), a larger temporal receptive field leads to better performance, emphasizing the importance of long-range temporal dependencies of speech for separation.
- (v) With the same configuration of the autoencoder, channels in the separation module ( $B$  and  $H$ ) and size of the receptive field, more convolutional blocks leads to better performance. This result suggests that stacking more convolutional blocks with smaller dilation factors is superior to fewer blocks with larger dilation factors having the same receptive field size.
- (vi) With the same number of filters  $N$  and separation module configuration, a smaller filter length  $L$  leads to better performance. Note that the best Conv-TasNet system uses a filter length of 2.5 ms ( $\frac{L}{f_s} = \frac{20}{8000} = 0.0025$  s), which makes it very difficult to train an LSTM separation module in [20], [54] with the same  $L$  due to the large number of time steps in the encoder output.
- (vii) With the same configuration of the entire network except for the type of normalization in the convolutional blocks, gLN has the best performance in the noncausal implementation, while BN has the best performance in the causal implementation. This result shows the importance of the normalization scheme and the difference between the causal and noncausal implementations.

### B. Comparison with other speech separation methods

Table III compares the performance of the proposed method with other state-of-the-art methods on the same WSJ0-2 mix dataset. For all systems, we list the best results that have been reported in the literature. The numbers of parameters in different methods are based on our implementations, except for [11], in which the network hyper-parameters are unspecified. The missing values in the table are either because the numbers were not reported in the study or because the results were calculated with a different STFT configuration. While the BLSTM-TasNet already outperforms the ideal ratio mask (IRM) and ideal binary mask (IBM), the noncausal Conv-TasNet significantly surpasses the performance of all three ideal time-frequency masks. Moreover, not only do both TasNet methods outperform all previous STFT-based systems, but also the separation is implemented in a purely end-to-end fashion, and the number of parameters is smaller.

Table IV compares the performance of the TasNet system with those of other systems on a three-speaker speech separation task involving the WSJ0-3mix dataset.

The noncausal Conv-TasNet system significantly outperforms all previous STFT-based systems. While there is no prior result on a causal algorithm for a three-speaker separation task, the causal Conv-TasNet significantly outperforms even the other two noncausal STFT-based systems [5], [6].

### C. Processing speed comparison

Figure V compares the processing speed of LSTM-TasNet and Conv-TasNet. The speed is evaluated as the average processing time for the systems to separate each frame in the mixtures, which we refer to as time per frame (TPF). TPF determines whether a system can be implemented in real time, which requires a TPF that is smaller than the frame length.

For the CPU configuration, we tested the system with one processor on a Intel Core i7-5820K CPU. For the GPU configuration, we preloaded both the systems and the data to a Nvidia Titan Xp GPU. LSTM-TasNet with CPU configuration has a TPF close to its frame length (5 ms), which is only marginally acceptable in applications where only a slower CPU is available. Moreover, the processing in LSTM-TasNet is done sequentially, which means that the processing of each time frame must wait for the completion of the previous time frame, further increasing the processing speed of the separation. Since Conv-TasNet decouples the processing of consecutive frames, the processing of subsequent frames does not have to wait until the completion of the current frame, which allows the possibility of parallel computing. This process leads to a TPF that is 5 times smaller than the frame length (2.5 ms) in our CPU configuration. Therefore, even with slower CPUs, Conv-TasNet can still perform real-time separation.

### D. Sensitivity of LSTM-TasNet to the mixture starting point

Unlike language processing tasks where sentences have determined starting words, it is difficult to define a general starting sample or frame for speech separation and enhancement tasks. A robust audio processing system should therefore be insensitive to the starting point of the mixture. However, we empirically found that the performance of the causal LSTM-TasNet is very sensitive to the exact starting point of the mixture, which means that shifting the input mixture by several samples may adversely affect the separation accuracy. We systematically examined the robustness of the causal LSTM-TasNet and Conv-TasNet to the starting point of the mixture by evaluating the separation accuracy for each mixture in the WSJ0-2mix test set with different sample shifts of the input. A shift of  $s$  samples corresponds to starting the separation at sample  $s$  instead of the first sample. Figure 4 A shows the performance of both systems on the same example mixture with different values of input shift. We observe that, unlike LSTM-TasNet, the causal Conv-TasNet performs consistently well for all shift values of the input mixture. We further tested the overall robustness for the entire test set by calculating the standard deviation of SDRi in each mixture with shifted mixture inputs similar to Figure 4 A. The box plots of all the mixtures in the WSJ0-2mix test set in Figure 4 B show

TABLE III  
COMPARISON WITH OTHER METHODS ON WSJ0-2MIX DATASET.

Method	# of param.	Causal	SI-SNRi (dB)	SDRi (dB)	PESQ
DPCL++ [5]	13.6M	×	10.8	–	–
uPIT-BLSTM-ST [6]	92.7M	×	–	10.0	–
DANet [7]	9.1M	×	10.5	–	2.64
ADANet [8]	9.1M	×	10.4	10.8	2.82
cuPIT-Grid-RD [55]	47.2M	×	–	10.2	–
CBLDNN-GAT[11]	–	×	–	11.0	–
Chimera++ [9]	32.9M	×	11.5	12.0	–
WA-MISI-5 [10]	32.9M	×	12.6	13.1	–
BLSTM-TasNet [54]	23.6M	×	13.2	13.6	3.04
<b>Conv-TasNet-gLN</b>	8.8M	×	<b>14.6</b>	<b>15.0</b>	<b>3.25</b>
uPIT-LSTM [6]	46.3M	✓	–	7.0	–
LSTM-TasNet [54]	32.0M	✓	<b>10.8</b>	<b>11.2</b>	2.84
<b>Conv-TasNet-BN</b>	8.8M	✓	<b>10.8</b>	<b>11.2</b>	<b>2.86</b>
Mixture	–	–	0	0	2.02
IRM	–	–	12.2	12.6	3.74
IBM	–	–	13.0	13.5	3.33
WFM	–	–	13.4	13.8	3.70

TABLE IV  
COMPARISON WITH OTHER SYSTEMS ON WSJ0-3MIX DATASET.

Method	# of param.	Causal	SI-SNRi (dB)	SDRi (dB)	PESQ
DPCL++ [5]	13.6M	×	7.1	–	–
uPIT-BLSTM-ST [6]	92.7M	×	–	7.7	–
DANet [7]	9.1M	×	8.6	8.9	1.92
ADANet [8]	9.1M	×	9.1	9.4	2.16
<b>Conv-TasNet-gLN</b>	8.9M	×	<b>11.6</b>	<b>12.0</b>	<b>2.50</b>
<b>Conv-TasNet-BN</b>	8.9M	✓	<b>7.7</b>	<b>8.1</b>	<b>2.08</b>
Mixture	–	–	0	0	1.66
IRM	–	–	12.5	13.0	3.52
IBM	–	–	13.2	13.6	2.91
WFM	–	–	13.6	14.0	3.45

TABLE V  
PROCESSING TIME FOR CAUSAL LSTM-TASNET AND CONV-TASNET.  
THE SPEED IS EVALUATED AS THE AVERAGE TIME REQUIRED TO  
SEPARATE A FRAME (TIME PER FRAME, TPF).

Method	CPU/GPU TPF (ms)
LSTM-TasNet	4.3/0.2
Conv-TasNet	<b>0.5/0.03</b>

that Conv-TasNet performs consistently better across the entire test set, which confirms the robustness of Conv-TasNet to variations in the starting point of the mixture.

### E. Properties of the basis functions

One of the motivations for replacing the STFT representation of the mixture signal with the convolutional encoder in TasNet was to construct a representation of the audio that is optimized for speech separation. To shed light on the properties of the encoder representation, we examined the basis functions of the decoder (rows of the matrix  $V$ ), as they form a linear transform back to the sound waveform. The basis functions are shown in Figure 5 for the best causal Conv-TasNet ( $L = 2.5$  ms), sorted by the similarity of the

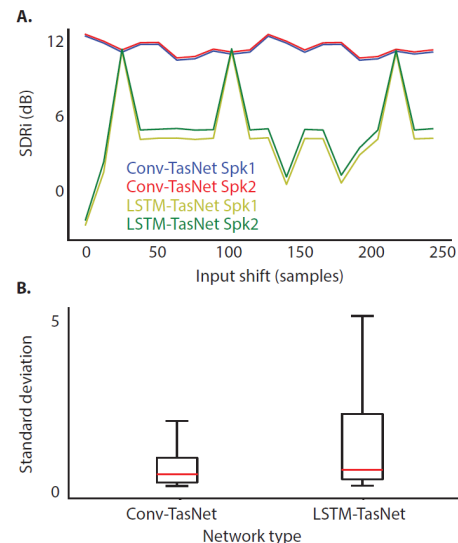


Fig. 4. (A): SDRi of an example mixture separated using the LSTM and Conv-TasNet models as a function of the starting point in the mixture. The performance of Conv-TasNet is considerably more consistent and insensitive to the start point. (B): Standard deviation of SDR improvements across all the mixtures in the WSJ0-2mix test set with varying starting points.

Euclidian distance of the basis functions similar to that in Figure 3. The magnitudes of the FFTs for each filter are also shown in the same order. As seen in the figure, the majority of the filters are tuned to lower frequencies. In addition, Figure 5 shows that filters with the same frequency tuning express all possible phase values for that frequency. This result suggests an important role for low-frequency features of speech such as pitch as well as explicit encoding of the phase information to achieve superior speech separation performance.

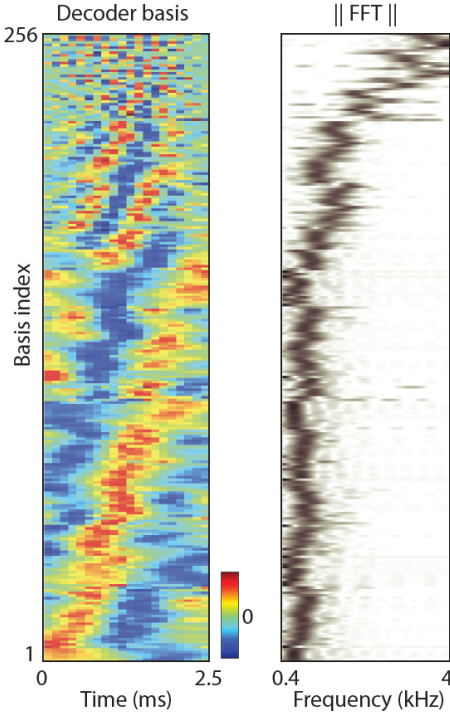


Fig. 5. Basis functions in the linear decoder and the magnitudes of their FFTs. The basis functions are sorted the same way as in Figure 3.

## VI. DISCUSSION

In this paper, we introduced the fully-convolutional time-domain audio separation network (Conv-TasNet), a deep learning framework for time-domain speech separation. TasNet is proposed to address the shortcomings of the STFT representation, namely the decoupling of phase and magnitude, the sub-optimal representation of the mixture audio for separation, and the high minimum latency of a STFT-based speech separation system. This improvement is accomplished by replacing the STFT with a convolutional autoencoder. The separation is done using a temporal convolutional network (TCN) architecture together with a depthwise separable convolution operation to address the challenges of LSTM networks. Our evaluations showed that Conv-TasNet significantly outperforms STFT speech separation systems even when the ideal time-frequency mask for the target speakers is used. In addition, TasNet has a smaller model size and a shorter minimum latency, which makes it suitable for low-resource, low latency applications.

Unlike STFT, which has a well-defined inverse transform that can perfectly reconstruct the input, a convolutional autoencoder does not guarantee that the input can be perfectly

reconstructed. The main reason is that the convolution and deconvolution operations of the autoencoder are not required to be exact inverse operations, unlike STFT and iSTFT operations. In addition, the ReLU nonlinearity of the encoder further prevents it from achieving perfect reconstruction. This rectification is necessary, however, for imposing a nonnegativity constraint on the encoder output, which is crucial for estimating the separation masks. If no constraint is imposed, the encoder output could be unbounded in which case a bounded mask cannot be properly defined. On the other hand, the ReLU activation used in the encoder implicitly enforces sparsity on the encoder output. Therefore, a larger number of basis functions is required to achieve an acceptable reconstruction accuracy compared with the linear STFT operation. This approach resembles an overcomplete dictionary in a sparse coding framework [33], [56] where each dictionary entry corresponds to a row in the decoder matrix  $\mathbf{V}$ .

The analysis of the encoder-decoder basis functions in Section V revealed two interesting properties. First, most of the filters are tuned to low acoustic frequencies (more than 60% tuned to frequencies below 1 kHz). This pattern of frequency representation, which we found using a data-driven method, roughly resembles the well-known mel frequency scale [57] as well as the tonotopic organization of the frequencies in the mammalian auditory system [58], [59]. In addition, the overexpression of lower frequencies may indicate the importance of accurate pitch tracking in speech separation, similar to what has been reported in human multitalker perception studies [60]. In addition, we found that filters with the same frequency tuning explicitly express all the possible phase variations. In contrast, this information is implicit in the STFT operations, where the real and imaginary parts only represent symmetric (cosine) and asymmetric (sine) phases, respectively. This explicit encoding of signal phase values may be the key reason for the superior performance of TasNet over the STFT-based separation methods.

The combination of high accuracy, short latency, and small model size makes Conv-TasNet a suitable choice for both offline and real-time, low-latency speech processing applications such as embedded systems and wearable hearing and telecommunication devices. Conv-TasNet can also serve as a front-end module for tandem systems in other audio processing tasks, such as multitalker speech recognition [61], [62], [63], [64] and speaker identification [65], [66]. On the other hand, several limitations of TasNet must be addressed before it can be actualized, including the long-term tracking of speakers and generalization to noisy and reverberant environments. Because Conv-TasNet uses a fixed temporal context length, the long-term tracking of an individual speaker may fail, particularly when there is a long pause in the mixture audio. In addition, the generalization of TasNet to noisy and reverberant conditions must be further tested [54], as time-domain approaches are more prone to temporal distortions, which are particularly severe in reverberant acoustic environments. In such conditions, extending the TasNet framework to incorporate multiple input audio channels may prove advantageous when more than one microphone is available. Previous studies have shown the benefit of extending speech separation to multichannel inputs

[67], [68], [69], particularly in adverse acoustic conditions and when the number of interfering speakers is large (e.g., more than 3).

In summary, TasNet represents a significant step toward the actualization of speech separation algorithms and opens many future research directions that would further improve its accuracy, speed, and computational cost, which could eventually make automatic speech separation a common and necessary feature of every speech processing technology designed for real-world applications.

## VII. ACKNOWLEDGMENTS

This work was funded by a grant from the National Institute of Health, NIDCD, DC014279; a National Science Foundation CAREER Award; and the Pew Charitable Trusts.

## REFERENCES

- [1] D. Wang and J. Chen, "Supervised speech separation based on deep learning: An overview," *IEEE/ACM Transactions on Audio, Speech, and Language Processing*, 2018.
- [2] X. Lu, Y. Tsao, S. Matsuda, and C. Hori, "Speech enhancement based on deep denoising autoencoder," in *Interspeech*, 2013, pp. 436–440.
- [3] Y. Xu, J. Du, L.-R. Dai, and C.-H. Lee, "An experimental study on speech enhancement based on deep neural networks," *IEEE Signal processing letters*, vol. 21, no. 1, pp. 65–68, 2014.
- [4] —, "A regression approach to speech enhancement based on deep neural networks," *IEEE/ACM Transactions on Audio, Speech and Language Processing (TASLP)*, vol. 23, no. 1, pp. 7–19, 2015.
- [5] Y. Isik, J. Le Roux, Z. Chen, S. Watanabe, and J. R. Hershey, "Single-channel multi-speaker separation using deep clustering," *Interspeech 2016*, pp. 545–549, 2016.
- [6] M. Kolbæk, D. Yu, Z.-H. Tan, and J. Jensen, "Multitalker speech separation with utterance-level permutation invariant training of deep recurrent neural networks," *IEEE/ACM Transactions on Audio, Speech, and Language Processing*, vol. 25, no. 10, pp. 1901–1913, 2017.
- [7] Z. Chen, Y. Luo, and N. Mesgarani, "Deep attractor network for single-microphone speaker separation," in *Acoustics, Speech and Signal Processing (ICASSP), 2017 IEEE International Conference on*. IEEE, 2017, pp. 246–250.
- [8] Y. Luo, Z. Chen, and N. Mesgarani, "Speaker-independent speech separation with deep attractor network," *IEEE/ACM Transactions on Audio, Speech, and Language Processing*, vol. 26, no. 4, pp. 787–796, 2018. [Online]. Available: <http://dx.doi.org/10.1109/TASLP.2018.2795749>
- [9] Z.-Q. Wang, J. Le Roux, and J. R. Hershey, "Alternative objective functions for deep clustering," in *Proc. IEEE International Conference on Acoustics, Speech and Signal Processing (ICASSP)*, 2018.
- [10] Z.-Q. Wang, J. L. Roux, D. Wang, and J. R. Hershey, "End-to-end speech separation with unfolded iterative phase reconstruction," *arXiv preprint arXiv:1804.10204*, 2018.
- [11] C. Li, L. Zhu, S. Xu, P. Gao, and B. Xu, "CBLDNN-based speaker-independent speech separation via generative adversarial training," in *Acoustics, Speech and Signal Processing (ICASSP), 2018 IEEE International Conference on*. IEEE, 2018.
- [12] D. Griffin and J. Lim, "Signal estimation from modified short-time fourier transform," *IEEE Transactions on Acoustics, Speech, and Signal Processing*, vol. 32, no. 2, pp. 236–243, 1984.
- [13] J. Le Roux, N. Ono, and S. Sagayama, "Explicit consistency constraints for stft spectrograms and their application to phase reconstruction," in *SAPA@ INTERSPEECH*, 2008, pp. 23–28.
- [14] Y. Luo, Z. Chen, J. R. Hershey, J. Le Roux, and N. Mesgarani, "Deep clustering and conventional networks for music separation: Stronger together," in *Acoustics, Speech and Signal Processing (ICASSP), 2017 IEEE International Conference on*. IEEE, 2017, pp. 61–65.
- [15] A. Jansson, E. Humphrey, N. Montecchio, R. Bittner, A. Kumar, and T. Weyde, "Singing voice separation with deep u-net convolutional networks," in *18th International Society for Music Information Retrieval Conference*, 2017, pp. 23–27.
- [16] S. Choi, A. Cichocki, H.-M. Park, and S.-Y. Lee, "Blind source separation and independent component analysis: A review," *Neural Information Processing-Letters and Reviews*, vol. 6, no. 1, pp. 1–57, 2005.
- [17] K. Yoshii, R. Tomioka, D. Mochihashi, and M. Goto, "Beyond nmf: Time-domain audio source separation without phase reconstruction," in *ISMIR*, 2013, pp. 369–374.
- [18] S. Venkataramani, J. Casebeer, and P. Smaragdīs, "End-to-end source separation with adaptive front-ends," *arXiv preprint arXiv:1705.02514*, 2017.
- [19] D. Stoller, S. Ewert, and S. Dixon, "Wave-u-net: A multi-scale neural network for end-to-end audio source separation," *arXiv preprint arXiv:1806.03185*, 2018.
- [20] Y. Luo and N. Mesgarani, "Tasnet: time-domain audio separation network for real-time, single-channel speech separation," in *Acoustics, Speech and Signal Processing (ICASSP), 2018 IEEE International Conference on*. IEEE, 2018.
- [21] F.-Y. Wang, C.-Y. Chi, T.-H. Chan, and Y. Wang, "Nonnegative least-correlated component analysis for separation of dependent sources by volume maximization," *IEEE transactions on pattern analysis and machine intelligence*, vol. 32, no. 5, pp. 875–888, 2010.
- [22] C. H. Ding, T. Li, and M. I. Jordan, "Convex and semi-nonnegative matrix factorizations," *IEEE transactions on pattern analysis and machine intelligence*, vol. 32, no. 1, pp. 45–55, 2010.

- [23] C. Lea, R. Vidal, A. Reiter, and G. D. Hager, "Temporal convolutional networks: A unified approach to action segmentation," in *European Conference on Computer Vision*. Springer, 2016, pp. 47–54.
- [24] C. L. M. D. F. René and V. A. R. G. D. Hager, "Temporal convolutional networks for action segmentation and detection," in *IEEE International Conference on Computer Vision (ICCV)*, 2017.
- [25] S. Bai, J. Z. Kolter, and V. Koltun, "An empirical evaluation of generic convolutional and recurrent networks for sequence modeling," *arXiv preprint arXiv:1803.01271*, 2018.
- [26] F. Chollet, "Xception: Deep learning with depthwise separable convolutions," *arXiv preprint*, 2016.
- [27] A. G. Howard, M. Zhu, B. Chen, D. Kalenichenko, W. Wang, T. Weyand, M. Andreetto, and H. Adam, "Mobilenets: Efficient convolutional neural networks for mobile vision applications," *arXiv preprint arXiv:1704.04861*, 2017.
- [28] D. Wang, "On ideal binary mask as the computational goal of auditory scene analysis," in *Speech separation by humans and machines*. Springer, 2005, pp. 181–197.
- [29] Y. Li and D. Wang, "On the optimality of ideal binary time–frequency masks," *Speech Communication*, vol. 51, no. 3, pp. 230–239, 2009.
- [30] Y. Wang, A. Narayanan, and D. Wang, "On training targets for supervised speech separation," *IEEE/ACM Transactions on Audio, Speech and Language Processing (TASLP)*, vol. 22, no. 12, pp. 1849–1858, 2014.
- [31] H. Erdogan, J. R. Hershey, S. Watanabe, and J. Le Roux, "Phase-sensitive and recognition-boosted speech separation using deep recurrent neural networks," in *Acoustics, Speech and Signal Processing (ICASSP), 2015 IEEE International Conference on*. IEEE, 2015, pp. 708–712.
- [32] A. Hyvriinen, "Survey on independent component analysis," *Neural Computing Surveys*, vol. 2, no. 4, pp. 94–128, 1999.
- [33] T.-W. Lee, M. S. Lewicki, M. Girolami, and T. J. Sejnowski, "Blind source separation of more sources than mixtures using overcomplete representations," *IEEE signal processing letters*, vol. 6, no. 4, pp. 87–90, 1999.
- [34] G.-J. Jang, T.-W. Lee, and Y.-H. Oh, "Single-channel signal separation using time-domain basis functions," *IEEE signal processing letters*, vol. 10, no. 6, pp. 168–171, 2003.
- [35] T. Kim, T. Eltoft, and T.-W. Lee, "Independent vector analysis: An extension of ica to multivariate components," in *International Conference on Independent Component Analysis and Signal Separation*. Springer, 2006, pp. 165–172.
- [36] Z. Koldovský and P. Tichavský, "Time-domain blind audio source separation using advanced ica methods," in *Eighth Annual Conference of the International Speech Communication Association*, 2007.
- [37] S. Makino, T.-W. Lee, and H. Sawada, *Blind speech separation*. Springer, 2007, vol. 615.
- [38] Z. Koldovsky and P. Tichavsky, "Time-domain blind separation of audio sources on the basis of a complete ica decomposition of an observation space," *IEEE Transactions on Audio, Speech, and Language Processing*, vol. 19, no. 2, pp. 406–416, 2011.
- [39] S.-W. Fu, T.-W. Wang, Y. Tsao, X. Lu, and H. Kawai, "End-to-end waveform utterance enhancement for direct evaluation metrics optimization by fully convolutional neural networks," *IEEE/ACM Transactions on Audio, Speech and Language Processing (TASLP)*, vol. 26, no. 9, pp. 1570–1584, 2018.
- [40] S. Pascual, A. Bonafonte, and J. Serrà, "Segan: Speech enhancement generative adversarial network," *Proc. Interspeech 2017*, pp. 3642–3646, 2017.
- [41] O. Ronneberger, P. Fischer, and T. Brox, "U-net: Convolutional networks for biomedical image segmentation," in *International Conference on Medical image computing and computer-assisted intervention*. Springer, 2015, pp. 234–241.
- [42] L. Kaiser, A. N. Gomez, and F. Chollet, "Depthwise separable convolutions for neural machine translation," *arXiv preprint arXiv:1706.03059*, 2017.
- [43] M. Sandler, A. Howard, M. Zhu, A. Zhmoginov, and L.-C. Chen, "Mobilenetv2: Inverted residuals and linear bottlenecks," in *Proceedings of the IEEE Conference on Computer Vision and Pattern Recognition*, 2018, pp. 4510–4520.
- [44] K. He, X. Zhang, S. Ren, and J. Sun, "Delving deep into rectifiers: Surpassing human-level performance on imagenet classification," in *Proceedings of the IEEE international conference on computer vision*, 2015, pp. 1026–1034.
- [45] —, "Deep residual learning for image recognition," in *Proceedings of the IEEE conference on computer vision and pattern recognition*, 2016, pp. 770–778.
- [46] J. L. Ba, J. R. Kiros, and G. E. Hinton, "Layer normalization," *arXiv preprint arXiv:1607.06450*, 2016.
- [47] S. Ioffe and C. Szegedy, "Batch normalization: Accelerating deep network training by reducing internal covariate shift," in *International Conference on Machine Learning*, 2015, pp. 448–456.
- [48] J. R. Hershey, Z. Chen, J. Le Roux, and S. Watanabe, "Deep clustering: Discriminative embeddings for segmentation and separation," in *Acoustics, Speech and Signal Processing (ICASSP), 2016 IEEE International Conference on*. IEEE, 2016, pp. 31–35.
- [49] "Script to generate the multi-speaker dataset using wsj0," <http://www.merl.com/demos/deep-clustering>.
- [50] D. Kingma and J. Ba, "Adam: A method for stochastic optimization," *arXiv preprint arXiv:1412.6980*, 2014.
- [51] E. Vincent, R. Gribonval, and C. Févotte, "Performance measurement in blind audio source separation," *IEEE transactions on audio, speech, and language processing*, vol. 14, no. 4, pp. 1462–1469, 2006.
- [52] A. W. Rix, J. G. Beerends, M. P. Hollier, and A. P. Hekstra, "Perceptual evaluation of speech quality (pesq)-a new method for speech quality assessment of telephone networks and codecs," in *Acoustics, Speech, and Signal Processing, 2001. Proceedings.(ICASSP'01). 2001 IEEE International Conference on*, vol. 2. IEEE, 2001, pp. 749–752.
- [53] L. E. Peterson, "K-nearest neighbor," *Scholarpedia*, vol. 4, no. 2, p. 1883, 2009.
- [54] Y. Luo and N. Mesgarani, "Real-time single-channel dereverberation and separation with time-domain audio separation network," *Proc. Interspeech 2018*, pp. 342–346, 2018.
- [55] C. Xu, X. Xiao, and H. Li, "Single channel speech separation with constrained utterance level permutation invariant training using grid lstm," in *Acoustics, Speech and Signal Processing (ICASSP), 2018 IEEE International Conference on*. IEEE, 2018.
- [56] M. Zibulevsky and B. A. Pearlmutter, "Blind source separation by sparse decomposition in a signal dictionary," *Neural computation*, vol. 13, no. 4, pp. 863–882, 2001.
- [57] S. Imai, "Cepstral analysis synthesis on the mel frequency scale," in *Acoustics, Speech, and Signal Processing, IEEE International Conference on ICASSP'83*, vol. 8. IEEE, 1983, pp. 93–96.
- [58] G. L. Romani, S. J. Williamson, and L. Kaufman, "Tonotopic organization of the human auditory cortex," *Science*, vol. 216, no. 4552, pp. 1339–1340, 1982.
- [59] C. Pantev, M. Hoke, B. Lutkenhoner, and K. Lehnertz, "Tonotopic organization of the auditory cortex: pitch versus frequency representation," *Science*, vol. 246, no. 4929, pp. 486–488, 1989.
- [60] C. J. Darwin, D. S. Brungart, and B. D. Simpson, "Effects of fundamental frequency and vocal-tract length changes on attention to one of two simultaneous talkers," *The Journal of the Acoustical Society of America*, vol. 114, no. 5, pp. 2913–2922, 2003.
- [61] J. R. Hershey, S. J. Rennie, P. A. Olsen, and T. T. Kristjansson, "Superhuman multi-talker speech recognition: A graphical modeling approach," *Computer Speech & Language*, vol. 24, no. 1, pp. 45–66, 2010.
- [62] C. Weng, D. Yu, M. L. Seltzer, and J. Droppo, "Deep neural networks for single-channel multi-talker speech recognition," *IEEE/ACM Transactions on Audio, Speech and Language Processing (TASLP)*, vol. 23, no. 10, pp. 1670–1679, 2015.
- [63] Y. Qian, X. Chang, and D. Yu, "Single-channel multi-talker speech recognition with permutation invariant training," *arXiv preprint arXiv:1707.06527*, 2017.
- [64] K. Ochi, N. Ono, S. Miyabe, and S. Makino, "Multi-talker speech recognition based on blind source separation with ad hoc microphone array using smartphones and cloud storage," in *INTERSPEECH*, 2016, pp. 3369–3373.
- [65] Y. Lei, N. Scheffer, L. Ferrer, and M. McLaren, "A novel scheme for speaker recognition using a phonetically-aware deep neural network," in *Acoustics, Speech and Signal Processing (ICASSP), 2014 IEEE International Conference on*. IEEE, 2014, pp. 1695–1699.
- [66] M. McLaren, Y. Lei, and L. Ferrer, "Advances in deep neural network approaches to speaker recognition," in *Acoustics, Speech and Signal Processing (ICASSP), 2015 IEEE International Conference on*. IEEE, 2015, pp. 4814–4818.
- [67] S. Gannot, E. Vincent, S. Markovich-Golan, A. Ozerov, S. Gannot, E. Vincent, S. Markovich-Golan, and A. Ozerov, "A consolidated perspective on multimicrophone speech enhancement and source separation," *IEEE/ACM Transactions on Audio, Speech and Language Processing (TASLP)*, vol. 25, no. 4, pp. 692–730, 2017.
- [68] Z. Chen, J. Li, X. Xiao, T. Yoshioka, H. Wang, Z. Wang, and Y. Gong, "Cracking the cocktail party problem by multi-beam deep attractor network," in *Automatic Speech Recognition and Understanding Workshop (ASRU), 2017 IEEE*. IEEE, 2017, pp. 437–444.

- [69] Z.-Q. Wang, J. Le Roux, and J. R. Hershey, "Multi-channel deep clustering: Discriminative spectral and spatial embeddings for speaker-independent speech separation," in *Acoustics, Speech and Signal Processing (ICASSP), 2018 IEEE International Conference on*. IEEE, 2018.